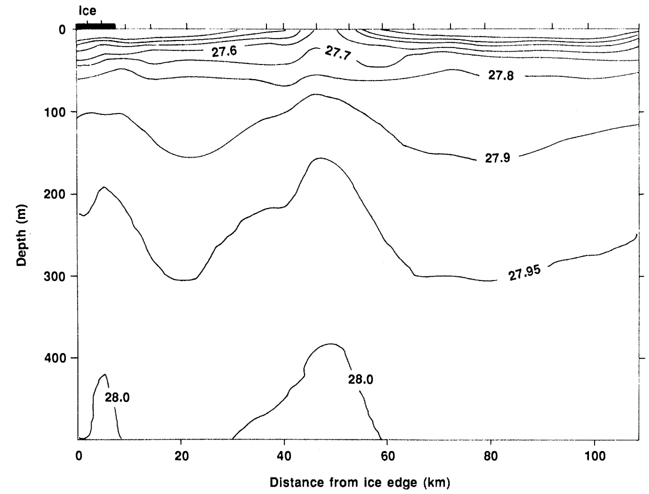

Fig. 3. Vertical density structure in the east-west direction perpendicular to the ice edge across eddy E1 near the center of the eddy. The units on the isopycnals are in $\Delta\rho t$.

that imaging radar can observe ice-ocean eddies even under high wind conditions. The ice convergence structure at the center reappeared when the wind decreased. The remote-sensing data showed that E1 had a lifetime of at least 20 days.

Extensive star pattern CTD sections of E1 obtained by the research vessels R.V. *Håkon Mosby* and R.V. *Kvitbjørn* during the period 10 to 14 July coupled with the remote-sensing observations during the same period give a nearly synoptic three-dimensional picture of the eddy. A section perpendicular to the ice edge (Fig. 3) near the center of E1 showed the doming and surfacing of the isopycnals, and indicated cyclonic motion down to 500 m and confirmed the rotation that was seen in the radar image. A CTD section in the north to south direction was obtained by R.V. *Polarstern* on 16 July and extended approximately 2500 m through to the bottom of E1. This section showed that E1 was actually present at depths of 800 to 1000 m. Measurements of current velocity within E1 (obtained by a satellite-tracked Argos buoy equipped with current meters) measured cyclonic orbital speeds of 30 to 40 cm/sec. The subsurface structures of E4 and E5 were also confirmed by CTD observations.

We could estimate the thermodynamic importance of eddies in determining the ice-edge position from the AVHRR image (Fig. 2). The cyclonic motion of each eddy not only swept ice away from the main ice pack but also transported warm Atlantic water (3° to 4°C) beneath the ice. Melt rates from the bottom of the ice tongue of E1 varied from 20 to 40 cm/day in contrast with rates of 2 to 3 cm/day when the ice was in the colder Arctic water. To estimate eddy thermodynamics, we assumed that half of the eddy was covered by ice and that the ice was 1.5 m thick; under such conditions the observed melt rates could easily account for the loss of approximately 350 km^2 of sea ice in 4 to 7 days. Hence at an eddy spacing of 50 km (Fig. 2), these eddies alone could cause the ice edge to melt at a rate of 1 to 2 km/day on average. Such intense melting was also observed from 1 to 6 June in the vicinity of the eddy E4 (*5*). The warming and thinning of the ice augmented by the eddies also made the ice more susceptible to fracturing by waves and floe collisions.

All of the eddies observed were cyclonic and were observed in an area of 3×10^5 km^2. They transferred heat from the warm Atlantic water to the ice and thus greatly enhanced the rates of ice melting. Eddies in the MIZ may play a more important role in transfer processes than eddies do in the temperate oceans. Both short- and long-forecasting models for range the ice edge position must include the effects of the eddies. Because of the close spacing of these eddies, our observations suggest that realistic MIZ models must include eddy-eddy interactions.

REFERENCES AND NOTES

1. O. M. Johannessen, J. A. Johannessen, J. Morison, B. Farrelly, E. Svendsen, *J. Geophys. Res.* **88**, 2755 (1983).
2. P. Wadhams and V. Squire, *ibid.*, p. 2770.
3. D. C. Smith, J. Morison, J. A. Johannessen, N. Untersteiner, *ibid.* **89**, 8205 (1984).
4. S. Hakkinen, thesis, Florida State University, Tallahassee (1984).
5. R. A. Shuchman *et al.*, *Science* **236**, 427 (1987).
6. This research was supported by the University of Bergen, the Royal Norwegian Council for Scientific and Industrial Research, the Norwegian Research Council for Science and Humanities, the U.S. Office of Naval Research (Arctic Programs), and the U.S. Geological Survey.

19 May 1986; accepted 14 January 1987

Remote Sensing of the Fram Strait Marginal Ice Zone

R. A. SHUCHMAN, B. A. BURNS, O. M. JOHANNESSEN,
E. G. JOSBERGER, W. J. CAMPBELL, T. O. MANLEY, N. LANNELONGUE

Sequential remote sensing images of the Fram Strait marginal ice zone played a key role in elucidating the complex interactions of the atmosphere, ocean, and sea ice. Analysis of a subset of these images covering a 1-week period provided quantitative data on the mesoscale ice morphology, including ice edge positions, ice concentrations, floe size distribution, and ice kinematics. The analysis showed that, under light to moderate wind conditions, the morphology of the marginal ice zone reflects the underlying ocean circulation. High-resolution radar observations showed the location and size of ocean eddies near the ice edge. Ice kinematics from sequential radar images revealed an ocean eddy beneath the interior pack ice that was verified by in situ oceanographic measurements.

A CENTRAL PROBLEM IN STUDIES OF the Fram Strait marginal ice zone (MIZ) is the definition of those mesoscale oceanic and atmospheric processes that determine the location of the ice edge, ice morphology, and ice deformation within the zone as well as the quantification of the major energy and momentum exchanges taking place there (*1*). Because marginal ice zones are located in regions that are either dark or cloudy for most of the year, microwave aircraft and satellite observations are the best means of obtaining high-resolution synoptic surface information. We present here an analysis of sequential high-resolution aircraft synthetic aperture radar (SAR) images from a region in the Fram Strait north of 79°N.

Figure 1 shows an SAR image obtained on 6 July 1984. This image, collected during total cloud cover from an altitude of 6.7 km,

R. A. Shuchman and B. A. Burns, Environmental Research Institute of Michigan, Ann Arbor, MI 48107.
O. M. Johannessen, Geophysical Institute–Nansen Ocean and Remote Sensing Center, University of Bergen, Bergen, Norway.
E. G. Josberger and W. J. Campbell, U.S. Geological Survey, Tacoma, WA 98416.
T. O. Manley, Lamont–Doherty Geological Observatory, Palisades, NY 10964.
N. Lannelongue, Centre National d'Études Spatiales, Toulouse, France.

has a spatial resolution of 3 m by 3 m that is independent of altitude. Resolution at this scale allows estimates of ice concentration accurate to 5%, a considerable improvement over radar estimates obtained earlier in the same area during the Norwegian Remote Sensing Experiment (*2*). Higher resolution increases the ability to identify individual floes and thereby provides more detailed ice kinematics. In Fig. 1 the ice edge is clearly delineated, as are polynyas (areas of open water or reduced ice concentration), ice floes varying in size from tens to hundreds of meters, ice concentrations of varying amounts, and the R.V. *Polarqueen*.

Figure 2 shows the results from an analysis of sequential aircraft images collected on 29 and 30 June and on 6 July 1984. Comparison of these images shows the transformation of a relatively north-south ice edge to a convoluted, meandering ice edge. These meanders result from the complex interactions along the boundary between the rapid southward East Greenland current, the warm northward-flowing Atlantic waters, and the highly variable winds (*3*). Ice edge meanders may play an important role in the generation of ice-ocean eddies (*4*) because they provide the initial perturbation in the Ekman transport field that eventually results in eddies. These edge features are composed of ice floes ranging from 50 to 500 m in size, which are the result of gravity wave–ice interaction and eddy-induced floe collisions that break up large floes. Under moderate wind conditions the ice in these meanders reflects the MIZ ocean circulation because the individual ice floes act as Lagrangian drifters moving with the current. This is particularly true in the summer season, when the winds are normally light (less than 4 m/sec) and there is no new ice forming that would freeze floes together.

The sequential images give ice drift kinematic data; the ice drift vectors (Fig. 2) were derived by locating the same floe in different images on 29 June and then on 6 July. The kinematic data reveal three regimes of floe drift during this 7-day period. First, the floes at the edge moved fastest, an average distance of 75 km (12.5 cm/sec), in a southwesterly direction, parallel to the ice edge. Second, floes west of 2°E, at distances greater than 40 km from the edge, moved approximately 45 km (7.5 cm/sec) to the south. Finally, in the region around the *Polarqueen* the ice drift was only 15 km (2.5 cm/sec) to the southwest.

The decrease in speed and the change in direction of the ice floe drift across the MIZ result from different forces acting on the ice in the interior and at the edge. The interior, with greater ice concentration and larger floes, is more strongly influenced by internal ice stress than the ice edge, which normally has lower ice concentrations and smaller floe sizes. The wind forcing also varies across the MIZ because the edge region, with smaller floe size and lower ice concentration, has a greater roughness than the interior. The third feature, the region of dramatically reduced ice drift, occurred at precisely the same time and location at which an ocean frontal meander was observed in the dynamic height topography produced by a helicopter-based conductivity, temperature, and depth (CTD) section (*5*). Furthermore, the drift of a sound fixing and ranging (SOFAR) buoy at a depth of 100 m (Fig. 2) through this anomalous ice drift area showed that this meander was a cyclonic ocean eddy. The location and size of this eddy was such that its circulation was opposed to the general ice drift direction,

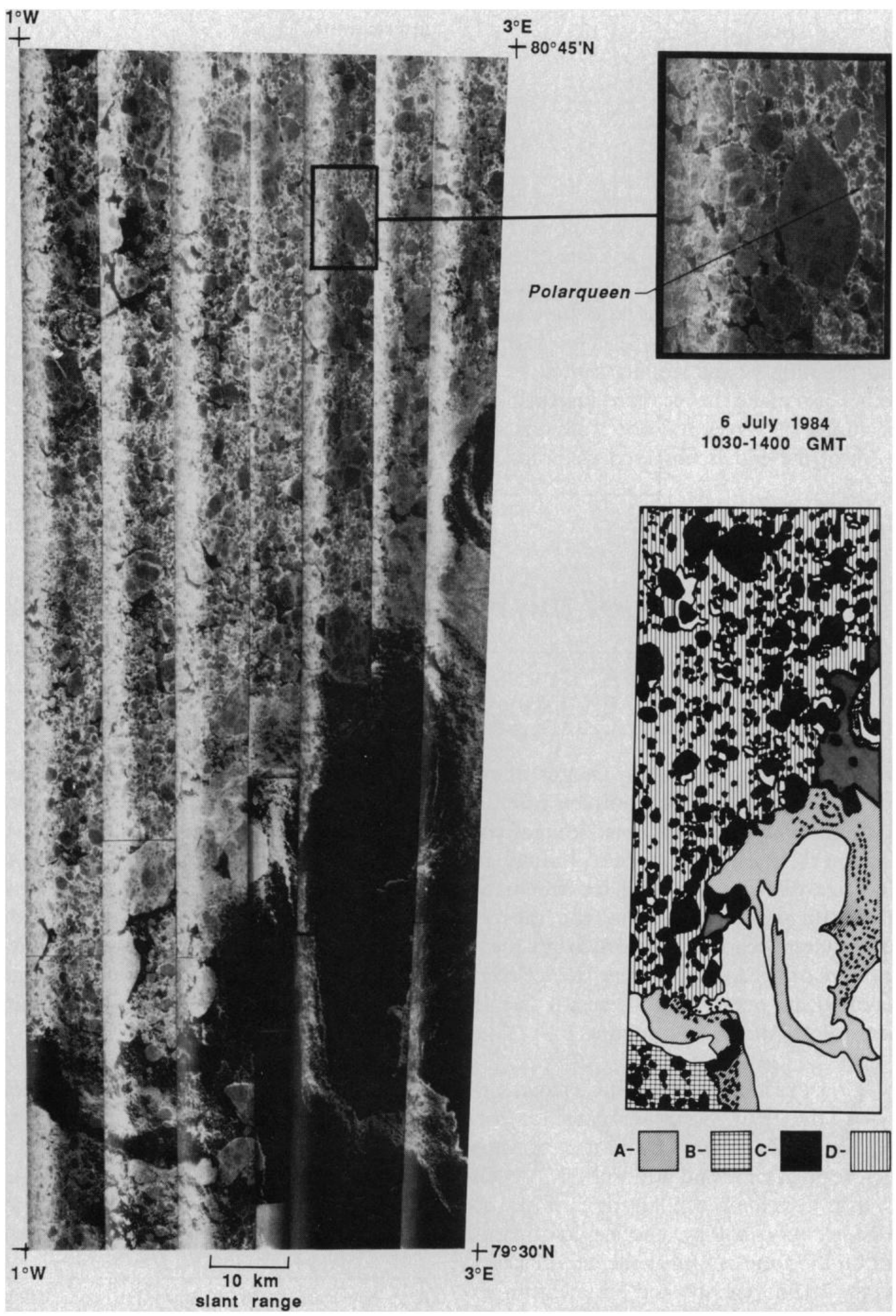

Fig. 1. L-band (23-cm) SAR imagery for 6 July. This image was obtained by the Environmental Research Institute of Michigan (ERIM) X-C- and L-band SAR mounted aboard the Canada Centre for Remote Sensing Convair 580 aircraft. The enlargement of the area around the *Polarqueen* shows the detailed ice information that a SAR can provide. In the interpretation solid black areas represent individual floes, and white areas represent ice-free ocean and polynyas. Areas A through D have the following ice concentrations, floe size ranges, and median floe sizes, respectively: (A) 20% to 45%, 8 to 500 m, and 125 m; (B) 45% to 70%, 0.5 to 2.5 km, and 1 km; (C) 70% to 90%, 8 to 500 m, and 100 m; (D) 80% to 100%, 10 m to 9 km, and 1 km.

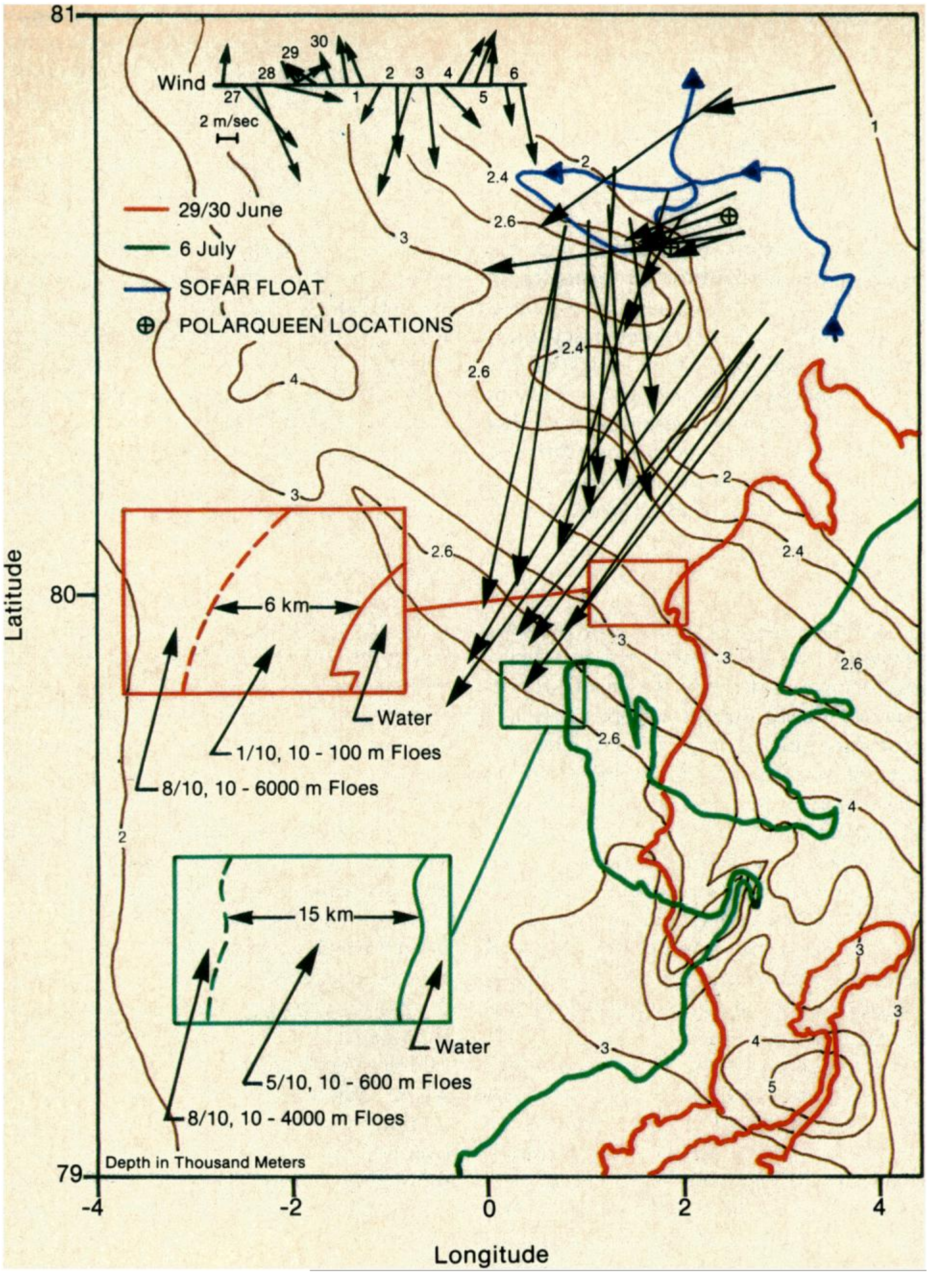

Fig. 2. Composite sketch of ice edge, concentration, and floe size for 29 and 30 June and for 6 July 1984 derived from remotely sensed data. Data from the ERIM SAR and the Centre National d'Études Spatiales B-17 Thompson VARVAN X-band side-looking airborne radar determined the ice edge position. The more detailed information about ice concentration and floe sizes were provided by the SAR as were the ice kinematics vectors which resulted from identifying individual ice floes and their positions. Also indicated on the figure are the track of a SOFAR buoy, bathymetry contours (fine brown lines), and local surface wind.

which reduced the ice drift velocities. Hence, the eddy slowed the ice drift in one region, changed the drift direction in the other region, and possibly augmented the drift to the north.

During this 7-day period, not only did the ice edge configuration change dramatically but so did the ice concentration distribution. On 29 and 30 June the first 6 km from the edge had a 10% concentration, and the remaining ice field had a concentration of 80% or greater. In contrast, the 6 July data show a 15-km-wide diffuse ice edge zone with an ice concentration of 50%, large floes close to the ice edge, and the region of 80% concentration farther from the edge caused by a northerly wind event from 2 to 4 July.

Ice advection and ablation control the ice edge position. For example, a 20-km southeasterly ice edge advance in the area between 80°20′N 4°E and 79°40′N 2°40′E on Fig. 2 was the result of ice advection from the northeast. The SAR-derived ice drift measurement of 75 km to the southwest near the ice edge confirms that the ice edge near 80°20′N 4°E on 30 June is the same ice edge near 79°40′N 2°40′E on 6 July and that ice was advected into this region from the northwest.

Bottom ablation measurements made in this region vary from almost 0 m/day when the ice is in cold Polar water to the very high value of 0.5 m/day when it comes in contact with warm (3° to 4°C) north Atlantic water. The disappearance of the ice meander at 79°20′N 3°E between 30 June and 6 July corroborates the ablation measurements and shows the importance of bottom ablation at the ice edge. This feature was visible on 29 and 30 June and had disappeared by 6 July (Fig. 2). The SAR-derived concentration measurements and areal coverage of the feature yielded a net ice area of approximately 500 km^2, and ice in this area is typically 2 m thick. The ice ablation measurements made in this region at the same time can easily account for the disappearance of the ice edge feature within a 6-day period.

In summary, these imaging radar observations show that the MIZ ice cover is highly variable and exhibits rapid dynamic and thermodynamic responses. At the ice edge, during light to moderate wind conditions, the ice drift mirrors the ocean circulation. The seaward migration of the ice edge, caused by either meandering ocean current or off-ice wind, is ultimately controlled by ice ablation. Radar-derived ice kinematics also provide information about ocean eddies beneath the ice in the interior of the MIZ. This information would be greatly improved by more frequent imaging of the MIZ, which would separate the advective from the temporal changes. These imaging radar aircraft observations show that forthcoming polar orbiting satellites with SAR, such as the European Research Satellite 1, can provide high-resolution (30-m) information about ice edge position, ice morphology, and ice kinematics that should allow us to achieve greater understanding of the complex interactions in the MIZ.

REFERENCES AND NOTES

1. O. M. Johannessen *et al.*, *Cold Regions Research and Engineering Laboratory Special Report 83-12* (U.S. Army Corps of Engineers, Hanover, NH, 1983).
2. NORSEX Group, *Science* **220**, 781 (1983).
3. O. M. Johannessen, J. A. Johannessen, S. Sandven, K. L. Davidson, in *The Environment of the Nordic Seas*, B. Hurdle, Ed. (Springer-Verlag, New York, 1986), pp. 665–679.
4. O. M. Johannessen *et al.*, *Science* **236**, 427 (1987).
5. T. Manley *et al.*, *ibid.*, p. 432.
6. We are grateful to the MIZEX Remote Sensing Group and other including C. Caruthers, J. C. Gascard, P. Gloersen, T. Grenfell, J. Hollinger, R. Jentz, J. A. Johannessen, M. Keller, C. Luther, J. Lyden, M. Mognaud, R. G. Onstott, D. Ross, C. Schgounn, L. L. Sutherland, and E. V. Vaillant, for comments, data, and help in preparing this manuscript. Supported by the Office of Naval Research, Arctic Program, under contracts N00014-81-C-0295 and N00014-83-C-0404.

19 May 1986; accepted 21 January 1987